CONF-870893--4

UCRL--96446

DE87 014250

FORMATION OF METASTABLE STRUCTURES AND AMORPHOUS PHASES IN PU-BASED SYSTEMS USING THE TRIODE TRIODE SPUTTERING TECHNIQUE

H.F. Rizzo, A.W. Echeverria,
W.L. Wien, and T.B. Massalski

This paper was prepared for submittal to the 6th International Conference on Rapidly Quenched Metals, Montreal, Canada.

August 3-7, 1987

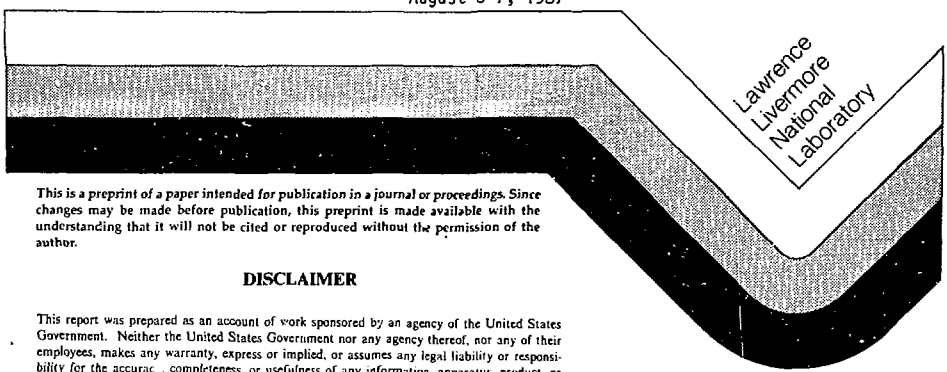

FORMATION OF METASTABLE STRUCTURES AND AMORPHOUS PHASES IN PU-BASED SYSTEMS USING THE TRIODE SPUTTERING TECHNIQUE.

H.F. Rizzo, A.W. Echeverria, W.L. Wien, and T.B. Massalski*

Lawrence Livermore National Laboratory, Livermore, CA 94550
*Carnegie Mellon University, Pittsburgh, PA 15213

The triode sputtering technique has been used to obtain metastable crystalline and amorphous phases in ten binary systems of Pu with Si, Al, V, Fe, Co, Pd, Ta, Re, Os, and Ir. The lattice parameters and near-neighbor distances evaluated with x-ray diffraction frequently show deviations from an assumed Vegard's Law which can be interpreted in relation to the changing electronic configuration and corresponding size of the Pu atom. When the Egami and Waseda [1] criterion is applied to predict the possible range of the amorphous phase formation, in terms of the atomic volume of the component atoms, the observed range exceeds the predicted range in Pu-rich alloys because the atomic size of the Pu atoms changes on alloying.

INTRODUCTION Metastable and amorphous alloys of Pu with the elements Mn, Fe, Co, Ni, Cu, Ru, Ti, Ga, and Ce have been prepared previously by the liquid quenching (LQ) technique [2,3] and by high rate sputtering with Ga, Ta, Ag, and Co [4,5,6]. Extended compositional ranges of Pu-amorphous alloys (Pu with Fe, Si, Ta [7] and Pu with Si, Al, V, Fe, Co, Pd, Ta, Re, Os, and Ir [8]) were prepared more recently with the triode sputtering technique.

Formation of glassy alloys by sputtering is not limited to eutectic regions in phase diagrams and can occur also in systems which have no eutectics, or display no solid solubility, or

involve compound formation. Figs. 1a and b for the Pu-Co and Pu-Ta systems illustrate these points. The ranges of glass formation are indicated underneath each diagram. Of particular interest in the present work is the minimum solute addition to Pu, in the ten Pu binary systems studied, that will result in glass formation. For this purpose, the experimentally determined minimum solute concentration C_B^{min} in Pu needed for the formation of an amorphous alloy was compared with the atomic size mismatch criterion developed by Egami and Waseda [1] and with results of recent studies of sputtered alloys by Liou and Chien [9].

EXPERIMENTAL Sputtered deposits of gradually changing composition were prepared by high-rate triode sputtering from a split-target of Pu and a selected solute element. A description of the triode sputtering system and procedures for depositing the Pu alloys on water-cooled (15-18°C) Al substrates (50.8 mm in diameter) is given in an earlier paper [7]. Deposition rates varied between 17 and 60 Å/s and deposits exceeding 300 microns were obtained. The Pu and solute elements used were 99.90 wt% pure. The composition across the entire surface (2.5-5.0 mm grid) of the sputtered deposit was determined using an x-ray EDS system.

X-ray diffraction patterns across the surface of the samples were obtained with a commercial Philips X-ray Diffractometer, using CuK_α radiation. Typical x-ray diffraction patterns shown in Fig. 2 are for Pu with 20 and 61 at.% Re alloys. These

broad low intensity peaks are characteristic of the amorphous structure. The width, (ß), at half height was used to estimate an "effective particle size", (D), in the material using the Scherrer formula [10], $\beta = \frac{.9\lambda}{D \cos \theta}$. The calculated D values for Pu-Re compositions varied between 12 and 14 Å, which is typical for the amorphous phases observed in the other nine systems which ranged between 10 and 29 Å.

An estimate of the average NNDs was also made for each system, using the Ehrenfest formula NND = K/K_1. Here K is a constant equal to about 7.9 ±1 (derived from a number of amorphous alloys) [11] and $K_1 = 4\pi \sin \theta/\lambda$. The uncertainty in the estimated NND values is ± .015 Å. Seitz radii were also calculated from NND values to compare with Seitz radii obtained from unit cells of crystalline structures. Seitz radius $r = (3\Omega/4\pi)^{1/3}$ can be derived from the volume per atom Ω in a unit cell of a given structure. The Seitz radii calculated from NND values involved the assumption that the amorphous phase volume is close-packed ($a_o^3 = 4\ \Omega$ and r = .553 NND). Additional details are discussed elsewhere [8].

RESULTS AND DISCUSSION A summary of phase regions, calculated NND values and atomic size ratios for the ten systems studied is presented in Table I. The overall range of amorphous compositions prepared by the present sputtering technique (10-77 at.% solute) is much wider than that produced by LQ techniques [2], which were limited between 10 and 30 at.% solute. The

ranges of amorphous phase obtained with sputtering, unlike the behavior of many LQ alloys, appear to have little to do with the form of the corresponding phase diagram (see Figs. 1a and b).

Analysis of the NND trends (presented in Table I in terms of composition) shows a wide variation in behavior for the different alloy systems. Most of the observed NND trends are reasonably linear. NND plots for Pu-Co and Pu-Ta systems are shown in Fig. 3. In order to emphasize interesting departures of NND values from any possible linear correlations between the pure elements involved, three NND values are shown for pure Pu, corresponding to the δ(fcc), ε(bcc), and the liquid phase extrapolated to room temperature. The decrease in Pu NND values from 3.28 Å (δ) to 3.095 Å (liq.) is generally believed to be due to the decrease in 5f electron localization.

Amorphous alloys of Pu with Co have NND values that are substantially above any linear relationship between Co and Pu (Fig. 3). The extrapolation suggests an expanded Pu atom. The large implied Pu radius in Pu-Co alloys suggests a change in the electronic configuration of Pu on alloying (i.e. an increased 5f localization) which was also noted in earlier work comparing sputtered amorphous alloys of $Pu_{11}Co_{89}$ (Pu_2Co_{17}) and $Sm_{11}Co_{89}$ [4]. The Pu-Fe alloys show similar trends to the Co alloys, but the extrapolation in Pu-rich region indicates an effective Pu radius as that in the ε phase of Pu, similarly to previously reported results for amorphous alloys prepared by LQ [2]. An extrapolation of NND data for the Pu-Ta alloys (Fig. 3) also indicates a Pu radius in the amorphous alloys corresponding

to that of ε-Pu. However, the NND values for the metastable bcc phase observed between 24 and 83 at% Ta fit within 1% of a linear Vegard's Law relationship between pure Ta and a slightly contracted liq-Pu form. The results for the Pu-V alloys are similar to those for Pu-Ta except that the metastable bcc phase was observed over a narrower range (55-62 at.% V).

Extrapolated NND data for Pu-Re, Pu-Os, and Pu-Ir amorphous alloys follow a linear relationship between the pure solute elements and indicate an effective Pu radius associated with an increasing amount of 5f localization. For example, Re alloys indicate a Pu radius corresponding to the c, Os alloys to δ, and Ir alloys to a radius above (+3%) that of δ-Pu.

Much more pronounced effects were observed for Pu with Pd, Al, and Si. Here, the initial size of the Pu atom in the amorphous range corresponds to ε-Pu in Pd and Si alloys and δ-Pu in Al alloys. On further alloying, the trend of NNDs remains far above any Vegard's Law type extrapolation in Pu-Al alloys and actually increases in Pu-Pd and Pu-Si alloys. Evidently a substantial localization of the 5f electrons is taking place, giving rise to a rather expanded size of Pu atoms. These effects are further amplified if the x-ray data are plotted in terms of calculated Seitz radii along with Seitz radii calculated from several equilibrium crystalline structures reported in the literature [12]. The contrast is particularly striking in the case of Pu-Pd alloys (Fig. 4) and with Pu-Ta alloys.

The atomic size mismatch between initial pure constituents, as used by Egami and Waseda [1] to predict the range of

amorphous phase formation was also examined for Pu systems studied. The proposed size-factor relationship related to atomic volumes is $|\lambda_o| \simeq C_B^{min}|\frac{\Delta V}{V_A}| \cong 0.1$, where λ_o is an empirical constant, V_A is the atomic volume of the solvent, ΔV is the volume difference between the solvent and the solute, and C_B^{min} is the minimum solute concentration needed for glass formation. Recently, Liou and Chien [9] estimated $|\lambda_o|$ to be in the range 0.07-0.09 for a large number of sputter-deposited binary alloys.

A comparison of the size ratios for the systems examined in the present study with the compositional ranges of amorphous phase formation is shown in Fig. 5 along with the range of expected amorphous phase compositions based on Egami and Weseda size factor relationship with an assumed $|\lambda_o|$ range of .07-.10. For purposes of the present calculations (Fig. 5), we used a Pu radius of 1.59 Å, (ε-Pu) and a twelve-coordination radius for the pure solute elements. In general, the agreement is reasonable, although in several systems for a given value of the radius ratio, the amorphous phase appears to form with even less solute than predicted. It must be assumed that electronic transfers between 5f and sd bands easily occur in such alloys of Pu. This can cause the effective radius ratio to be much larger than assumed, leading to a further extension of the possible amorphous range towards pure Pu, as observed.

ACKNOWLEDGEMENTS The authors are grateful to P. Wallace and D. DelGuidice for x-ray and microprobe analyses and one of us (T.B.M.) gratefully acknowledges partial support from the

National Science Foundation (DMR Grant No. 84-12989). This work was performed under the auspices of the U.S. Dept. of Energy by the Lawrence Livermore National Laboratory under Contract No. W-7405-Eng-48.

REFERENCES

1. T. Egami and Y. Waseda, J. Non-Cryst. Solids 64, 113 (1984).

2. R.O. Elliott and B.C. Giessen, Acta Metallurgica 30, 785 (1982).

3. R.O. Elliott and B.C. Giessen, in Plutonium and Other Actinides, H. Blank and R. Linder, Eds. (North-Holland, Amsterdam, 1976), p. 47.

4. R.P. Allen, S.P. Dahlgren and R. Wang, in Plutonium and Other Actinides, H. Blank and R. Linder, Eds. (North-Holland, Amsterdam, 1976), p. 61.

5. R.A. Busch, in Plutonium 1970 and Other Actinides, W.N. Miner, Ed., (AIME, New York, 1970), p. 1045.

6. R.A. Busch, in Plutonium 1970 and Other Actinides, W.N. Miner, Ed., (AIME, New York, 1970), p. 1037.

7. H.F. Rizzo and A.W. Echeverria, J. Less Common Metals, 121(1986), p. 469.

8. H.F. Rizzo, T.B. Massalski, and A.W. Echeverria, submitted to AIME Trans.

9. S.H. Liou and C.L. Chien, Phys. Rev. B, 35 (5). 2443, (1987).

10. C.S. Barrett and T.B. Massalski, Structure of Metals (Pergamon Press, Oxford, England, 1980), 3rd ed., p. 155.

11. B.C. Giessen and C.N.J. Wagner, in Liquid Metals, (Ed. S.Z. Beer), M. Dekker, New York, 1972, p. 654.

12. P. Villars and L.D. Calvert, Eds. Pearson's Handbook of Crystallographic Data for Intermetallic Phases, Vol. II & III (ASM, Ohio, 1985).

13. F.H. Ellinger, W.N. Miner, D.R. O'Boyle, and F.W. Schonfeld, Constitution of Plutonium Alloys, Los Alamos National Laboratory, Los Alamos, NM, LA-3870 (1968)

14. L.J. Wittenberg and R. DeWitt, J. Chem. Phys. 56,9, 4526 (1972).

15. Unpublished results.

Fig. 1a-b. Compositional ranges and phases found in sputtered deposits displayed below the binary Pu-Co and Pu-Ta phase diagrams [13].

Fig. 2. XRD patterns from sputtered Pu-Re deposits varying in composition between 20 and 61 at.% Re.

Fig. 3. Calculated nearest neighbor distances (NND) obtained from sputtered Pu-Co amorphous, Pu-Ta amorphous, and bcc Ta-Pu alloys. NND values for pure Pu are shown for the fcc δ-phase and the bcc ε-phase at room temperature. A hypothetical value of NND in Pu liquid at RT is also shown, based on extrapolation of the thermal expansion observed in the liquid range [14].

Fig. 4. Calculated Seitz radii obtained from sputtered Pu amorphous alloys with Pd and Ta. Seitz radii are shown for fcc δ, bcc ε, liquid Pu and crystalline Pd, Ta, and Pu-Pd compounds.

Fig. 5. Calculated minimum solute composition at which the formation of the amorphous phase is expected (based on Egami-Weseda relationship with $|\lambda_0| = .07-.10$) with superimposed experimental data from this study and refs. [9,15].

00910

Table I

Summary of phases observed for sputtered Pu alloys and calculated NND values

SYSTEM	SPUTTERED SOLUTE RANGE at %	AMORPHOUS RANGE & Calculated NNDs atomic %	Å	CRYSTALLINE PHASE (RANGE)	$\frac{r^*_{Pu}}{r^{**}_{solute}}$ (ratio)
Pu-V	12-62	12-62	3.18-3.10	ε (55-62)	1.18
Pu-Tc	22-83	22-50	3.13-3.05	ε (24-83)	1.11
Pu-Fe	13-75	13-75	3.14-2.87	Pu_6Fe (13-25)	1.25
Pu-Co	18-69	18-69	3.28-2.95	Pu_6Co (18-25) "$CaCu_5$" (63-69)	1.27
Pu-Re	20-61	20-61	3.08-2.93	none	1.16
Pu-Os	20-70	20-70	3.17-2.95	none	1.18
Pu-Ir	21-77	21-77	3.26-2.82	$PuIr_2$ (65-77)	1.17
Pu-Al	10-63	18-63	3.26-3.19	δ (8-32)	1.11
Pu-Si	10-58	10-58	3.18-3.32	Pu_3Si_2 (trace 32-50)	1.20
Pu-Pd	7-52	17-50	3.23-3.28	β–Pu (7-17) PuPd (42-50)	1.16

* Pu radius = 1.59 Å

** Solute radii correspond to 12 coordination close packed structures

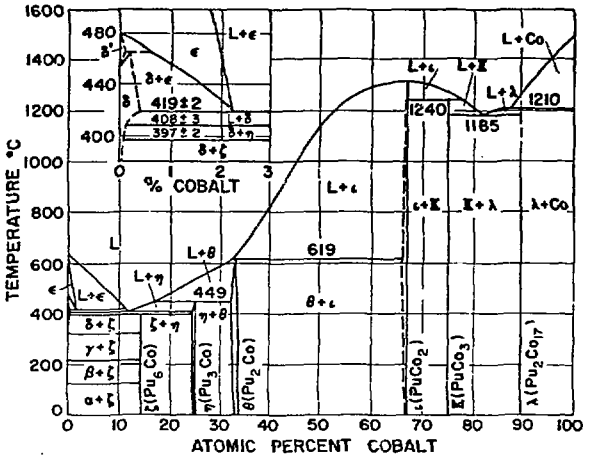

(a)

amorphous

mixed phases

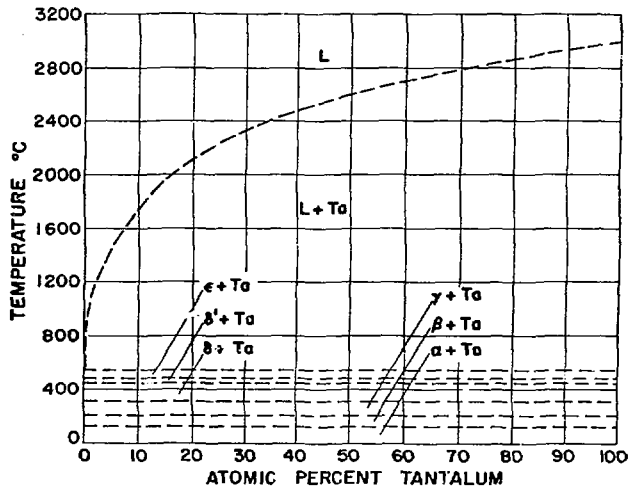

(b)

BCC

Figure 1

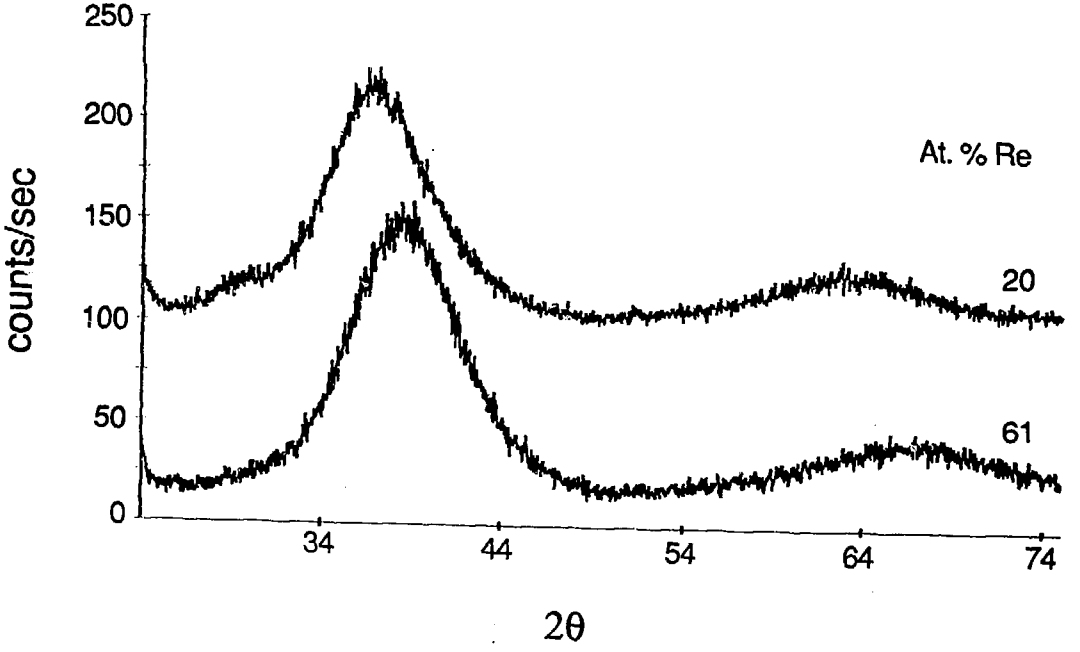

Figure 2

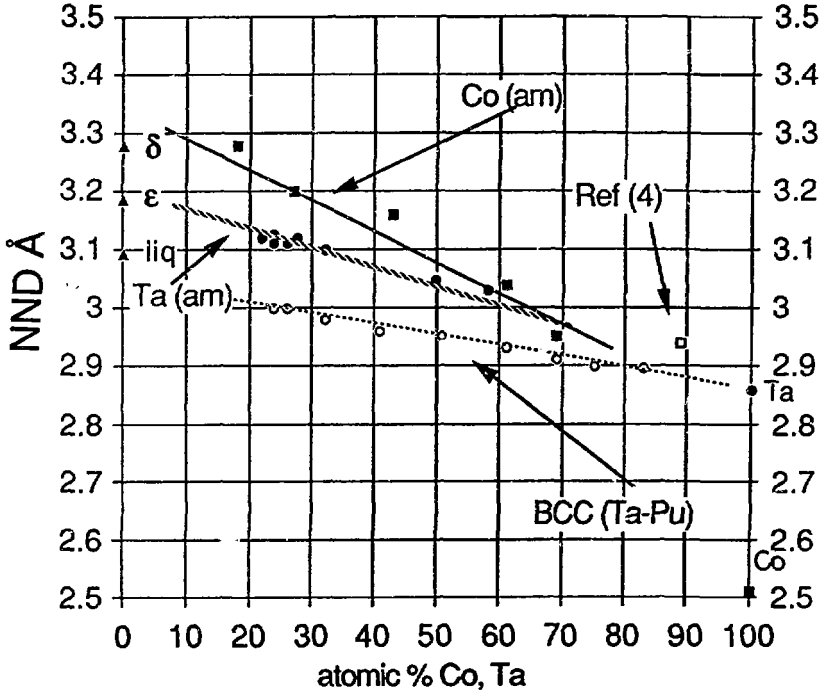
NND Å
3.5
3.4
3.3
3.2
3.1
3
2.9
2.8
2.7
2.6
2.5
δ
ε
liq
Co (am)
Ref (4)
Ta (am)
Ta
BCC (Ta-Pu)
Co
0 10 20 30 40 50 60 70 80 90 100
atomic % Co, Ta

Figure 3

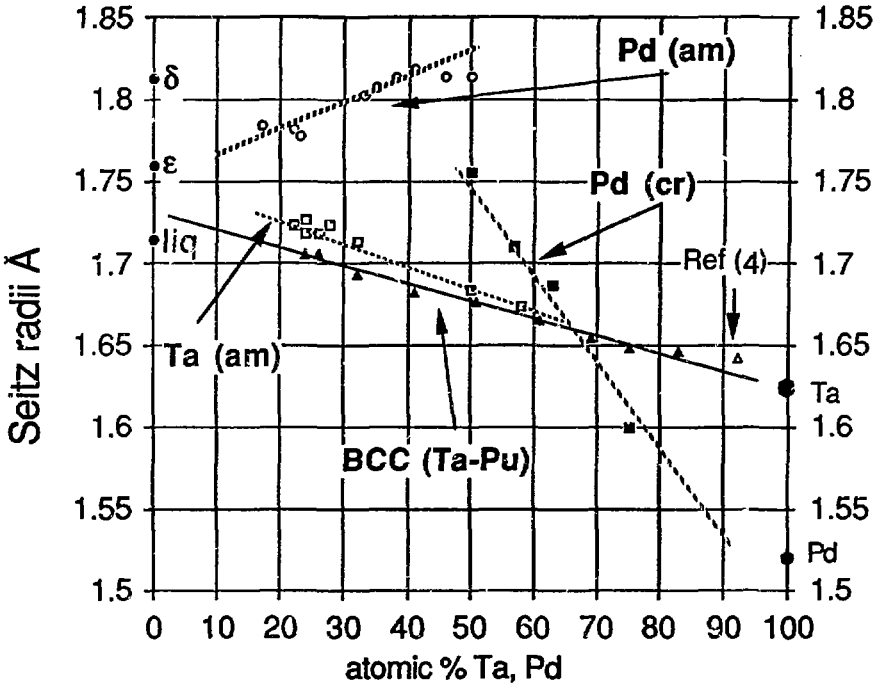
Seitz radii Å
1.85
1.8
1.75
1.7
1.65
1.6
1.55
1.5
δ
ε
liq
Pd (am)
Pd (cr)
Ref (4)
Ta (am)
BCC (Ta-Pu)
Ta
Pd
0 10 20 30 40 50 60 70 80 90 100
atomic % Ta, Pd

Figure 4

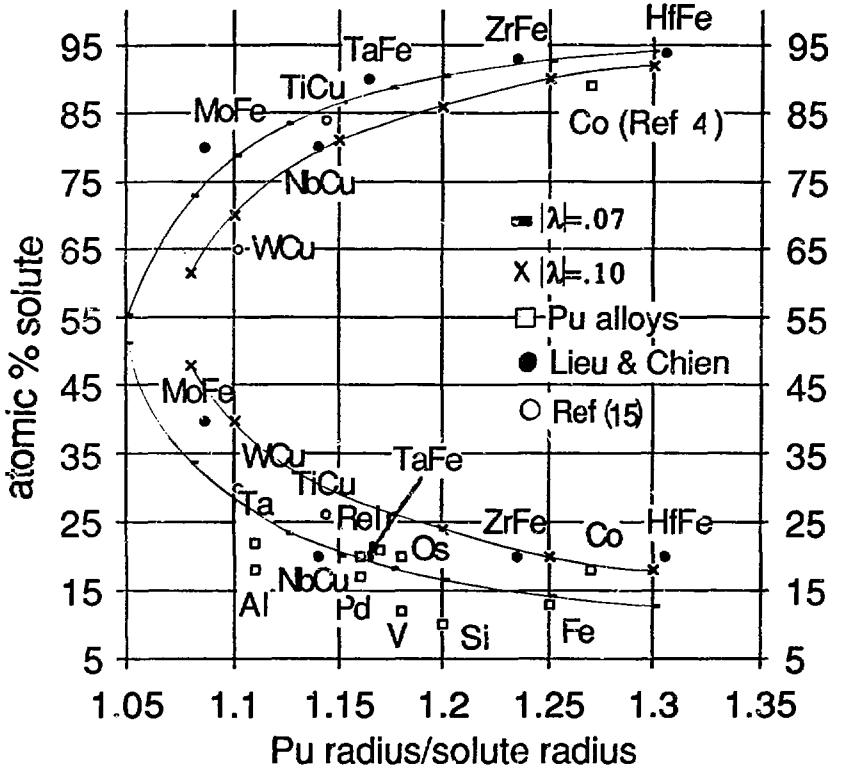
atomic % solute
Pu radius/solute radius
95
85
75
65
55
45
35
25
15
5
1.05
1.1
1.15
1.2
1.25
1.3
1.35
HfFe
ZrFe
TaFe
TiCu
MoFe
Co (Ref 4)
NbCu
WCu
|λ|=.07
|λ|=.10
Pu alloys
Lieu & Chien
Ref (15)
MoFe
WCu
TaFe
TiCu
Ta
ReI
ZrFe
Co
HfFe
Os
NbCu
Al
Pd
V
Si
Fe

Figure 5